Ceramics International 52 (2026) 6430–6441

Contents lists available at ScienceDirect

Ceramics International

journal homepage: www.elsevier.com/locate/ceramint

Dual-functional cerium-containing mesoporous bioactive glasses for drug delivery

Chiara Cavazzoli [a], Roberta Salvatori [b], Alexandre Anesi [b], Alfonso Zambon [a,*], Gigliola Lusvardi [a,**]

[a] Department of Chemical and Geological Sciences, University of Modena and Reggio Emilia, 41125, Modena, Italy
[b] Biomaterials Laboratory, Department of Medical and Surgical Sciences for Adults and Children, University of Modena and Reggio Emilia, 41125, Modena, Italy

ARTICLE INFO

Keywords:
Glasses
Cerium
Co-loading
Antioxidants
Bioactivity
Cytocompatibility

ABSTRACT

Cerium-doped mesoporous bioactive glasses were synthesized and individually loaded with polyphenols (quercetin, 3-hydroxyflavone, morin hydrate and a natural mixture) and common drugs (ibuprofen and paracetamol). The resulting materials were then combined in a 1:1 wt ratio to exploit their complementary therapeutic functionalities.

The antioxidant activity of the dual-loaded systems was assessed through enzymatic assays, revealing a clear synergistic effect between cerium and polyphenols; this interaction endowed the materials with highly effective and stable antioxidant properties, which remained unaffected by the simultaneous presence of the drugs.

In vitro bioactivity tests confirmed the ability of the dual-loaded systems to promote the formation of an apatite layer, indicative of their osteoconductive potential; this mineralization process was slightly delayed as a consequence of the dual loading and cerium incorporation.

Cytocompatibility assays performed with relevant cell models demonstrated the biocompatibility of all formulations, with particularly promising outcomes for the systems combining cerium, ibuprofen, and quercetin.

These findings highlight the potential of these newly developed dual-loaded systems for biomedical applications requiring both antioxidant protection and sustained bioactivity, such as bone tissue regeneration or therapies targeting inflammation-prone environments.

1. Introduction

Bioceramics, and in particular bioactive glasses (BGs), are widely used in biomedical applications, such as bone fillers, scaffolds, and implant coatings due to their capacity to promote hard tissue regeneration [1–3].

Recent research has focused on enhancing the biological performance of BGs by doping them with therapeutic inorganic ions (TIIs), such as cerium, known for its antioxidant, antiemetic, bacteriostatic, and anticancer properties [3–7]. Moreover, BGs can be functionalized with organic molecules, including biomolecules and drugs, to develop advanced drug delivery systems (DDSs) [8–10].

Our previous studies [7,11] have demonstrated that cerium-doped BGs (BGsCe) retain their bioactivity while exhibiting significant antioxidant properties, notably mimicking catalase (CAT) and superoxide dismutase (SOD) enzymatic activity. These features make BGsCe promising candidates for reducing post-implantation inflammation and mitigating reactive oxygen species (ROS)-induced damage.

Moreover, in vivo studies demonstrated that our BGsCe enhance cellular compatibility and support long-term bone remodelling, leading to a more controlled and efficient healing process compared with cerium-free BGs [12].

Advances in synthesis methods have improved the performance of traditionally produced BGs, leading to the development of mesoporous bioactive glasses (MBGs). Thanks to their high pore volume, large specific surface area (SSA), and ordered mesostructure, these materials allow the efficient loading and controlled release of biomolecules [3,13,14].

Among biomolecules, natural polyphenols have attracted increasing interest because of their antioxidant, anti-inflammatory, antibacterial, osteoinductive, and antitumor properties [15–19].

Our research group has developed solid expertise in the design and

* Corresponding author.
** Corresponding author.
E-mail addresses: alfonso.zambon@unimore.it (A. Zambon), gigliola.lusvardi@unimore.it (G. Lusvardi).

https://doi.org/10.1016/j.ceramint.2025.12.397
Received 20 October 2025; Received in revised form 11 December 2025; Accepted 25 December 2025
Available online 26 December 2025

characterization of cerium-doped MBGs (MBGsCe) loaded with various polyphenols, including quercetin (Q), 3-hydroxyflavone (F), morin hydrate (M), and a polyphenolic mixture extracted from chestnut flour (C) [11,13,20–22].

Previous studies have confirmed the successful loading of these biomolecules onto MBGsCe, while preserving the mesoporous structure. They also demonstrated an enhancement in antioxidant performance, particularly regarding SOD-like activity, which is otherwise absent in unloaded glasses [11,20]. Furthermore, the combination of cerium doping (key for CAT-like activity) and polyphenol loading (responsible for SOD-like activity) resulted in complementary and highly effective antioxidant functionality.

These properties were also retained in more complex systems, such as hydrogels containing MBGsCe, confirming their versatility and potential applications not only in hard tissue regeneration but also in soft tissues, for example in wound healing [21]. We also demonstrated that a dual-loaded system (1:1 mixture of MBGsCe separately loaded with gentamicin and natural polyphenolic mixture type-C) [13] preserves bioactivity and exhibits antioxidant and antibacterial properties.

Therefore, we decided to extend the study to additional drugs and polyphenols, with the aim of developing new dual-loaded systems capable of harnessing their complementary therapeutic effects.

To this end, we selected widely used drugs such as ibuprofen (IBU) and paracetamol (PARA), while among the polyphenols we included C again, as well as Q, F, and M.

IBU is a non-steroidal anti-inflammatory drug (NSAID) that inhibits prostaglandin synthesis by blocking cyclooxygenase enzymes (Cox-1 and Cox-2). As a propionic acid derivative, it exerts analgesic, anti-inflammatory, and antipyretic effects, and is widely used to treat conditions such as rheumatoid and juvenile arthritis [23,24]. PARA, by contrast, is one of the most widely used medications for the management of pain and fever. Unlike NSAIDs, it lacks anti-inflammatory properties, but is characterized by an excellent safety profile and versatility, making it a reference analgesic and antipyretic for both adults and children [25,26].

Therefore, in this study, the new dual-loaded MBGsCe systems were evaluated to determine their drug loading efficiency, antioxidant properties (enzymatic assay), bioactivity (in vitro studies), and cytotoxicity (according to ISO 10993-5 guidelines) [27–29].

2. Materials and methods

2.1. MBGsCe preparation and biomolecules' loading

MBGsCe, with the composition SiO_2-CaO-P_2O_5-$(CeO_2)_x$ (x = 0 and 3.6 mol%), were synthesized via the sol-gel EISA method as described in our previous studies [3,11,20], and subsequently sieved to obtain powders in the 212–355 μm size range. The experimental composition is reported in Table S1.

The 1.0 mg/mL polyphenol loading solutions were prepared using the following polyphenols: C and Q, F and M with purities of 95, 98, and 100 % respectively. C was dissolved in bidistilled water, whereas Q, F, and M were dissolved in ethanol under magnetic stirring for 1 h.

The loading process involved soaking 0.1 g of MBGsCe in 5 mL of the loading solutions at 37 °C for 3 h. To minimize light exposure, all samples were wrapped in aluminium foil [11,20].

A 2 mg/mL IBU solution was prepared by dissolving the drug in heptane under magnetic stirring for 30 min, followed by immersion of 0.1 g of MBGsCe in 10 mL of the solution at 25 °C for 6 h. Similarly, a 5 mg/mL PARA solution was prepared in ethanol, and loading was carried out by soaking 0.1 g of MBGsCe in 20 mL of the solution at 25 °C for 24 h.

To obtain the dual-loaded systems, MBGsCe powders separately loaded with polyphenols and drugs were mixed in a 1:1 wt ratio.

The resulting 16 samples are referred to as "MBGsCe–polyphenol–drug", where Ce = 0 or 3.6 mol%; polyphenol = Q, F, M or C; and drug = IBU or PARA.

2.1.1. Elemental analyses (AE)

Elemental analysis (EA) was performed using a FLASH 2000 Thermo Fisher analyser to quantify the biomolecules loaded onto the MBGsCe by measuring the carbon content (%C). The results for each biomolecule are expressed as loading content (LC, %) and loading efficiency (LE, %), calculated as follows, where *m* represents mass. All values are based on three replicate experiments.

$$LC(\%) = \frac{MM(biomolecule)}{n^o\ of\ C\ (C\ into\ biomolecule)\ x\ MA(C)} \times C(\%)$$

$$LE(\%)^* = \frac{m_{(biomolecule\ loaded)}{}^*}{m\ (biomolecule\ loading\ solution)} \times 100$$

* Derived from LC (%).

2.1.2. SSA determination

SSA was evaluated before and after loading to assess possible textural changes resulting from the process. SSA was determined by nitrogen adsorption using a Micromeritics Chemisorb 2750 porosimeter and the Brunauer–Emmett–Teller (BET) method [30].

2.2. Antioxidant activity assay

The antioxidant properties of each dual-loaded system were evaluated through enzymatic assays to assess their ability to scavenge hydrogen peroxide (H_2O_2) and the superoxide radical anion ($O_2^{\cdot-}$), two of the most relevant ROS [3,31–33].

2.2.1. CAT-like activity

The tests were performed using the Fluorimetric Hydrogen Peroxide Assay Kit (Sigma Aldrich) and a TECAN GeniosPro microplate reader, as described in our previous study [11]. The presence of H_2O_2 in DPBS (Dulbecco's Phosphate Buffered Saline, D8537) was detected through its 1:1 stoichiometric reaction with a molecular probe, catalyzed by the peroxidase, which generates a red-fluorescent product detectable fluorometrically. Each dual-loaded system (40 mg) was suspended in 400 μL of a 50 μM H_2O_2 solution in DPBS, and the residual H_2O_2 concentration was measured using the Amplex assay after 30 and 120 min of soaking. CAT activity is expressed as the percentage of H_2O_2 decomposed at the end of the assay.

2.2.2. SOD-like activity

The tests were performed using the SOD Determination Kit (Sigma Aldrich) adapted for the use with a UV–Vis spectrophotometer (JASCO V-770, Mettler Toledo, Columbus, Ohio, United States) [11].

The assay was conducted on both powders and soaking solutions after 1, 4, 24 and 48 h of immersion in DPBS, using a glass-to-DPBS ratio of 75mg/50 mL. DPBS was used to simulate the physiological environment in which these materials are intended to operate.

In this assay, SOD-like activity is expressed as the inhibition rate (I.R. %) of the formation of a water-soluble formazan dye. This dye is produced by the reduction of a tetrazolium salt (WST-1) by the superoxide anion, a process catalyzed by xanthine oxidase (XO) and inhibited by SOD.

2.3. In vitro bioactivity assessment

All dual-loaded MBGsCe were soaked in simulated body fluid (SBF) [34–37] at 37 °C for 7 and 14 days to assess the formation of an apatite layer, primarily composed of $Ca_{10}(PO_4)_6(OH)_2$ (hydroxyapatite, HA) which indicates the bioactivity of the materials even after biomolecules loading.

After soaking, the samples were characterized by:

- X-Ray Powder Diffraction (XRPD), using an Empyrean MultiCore 3rd generation diffractometer (Malvern Panalytical, Malvern, United Kingdom) to verify the presence of crystalline HA;
- Scanning Electron Microscopy (SEM) with a JEOL JSM-6010LA microscope (equipped with Electron Dispersive Spectroscopy, EDS, Leica Microsystems Wetzlar, Germany) to evaluate morphological changes on the surface;
- Fourier Transform Infrared (FTIR) spectroscopy with a Perkin Elmer FT-IR 160 spectrometer (Waltham, Massachusetts, United States) to identify characteristic bands of HA.

2.4. Cytocompatibility assays

2.4.1. Sample preparation

Cytocompatibility was evaluated in accordance with ISO 10993-5 guidelines [12,22,27,28,38–41].

Samples were tested using both the Neutral Red (NR) and the 3-(4,5-dimethyl-2-thiazolyl)-2,5-diphenyl-2H-tetrazolium bromide (MTT) assays.

MLO-Y4 cells (murine long bone osteocytes-like cells obtained from the Istituto Zooprofilattico Sperimentale, IZS Brescia, Italy) were used for the evaluation.

Cells were cultured in Dulbecco's Modified Eagle Medium (DMEM; Euroclone, Milan, Italy) supplemented with 10 % fetal bovine serum, 100 μg/mL penicillin-streptomycin, and 1 mM sodium pyruvate (all from Euroclone, Milan, Italy).

Cultures were maintained at 37 ± 1 °C in a humidified atmosphere with 5 ± 1 % CO_2 in air. Prior to testing, samples were sterilized by autoclaving at 121 °C.

2.4.2. Neutral Red (NR) assay

The Neutral Red (NR) assay is a well-established method for assessing cell viability. It measures the uptake of NR dye (N2889, Sigma-Merck, Darmstadt, Germany), which penetrates intact cell membranes and accumulates in the lysosomes of viable cells, thus indicating both membrane integrity and lysosomal functionality. According to ISO 10993-5 guidelines [27–29], the samples were directly applied to cells at a ratio of 10 mg/mL.

Cells were seeded in 12-well plates and cultured at 37 ± 1 °C, with 90 ± 5 % humidity and 5 ± 1 % CO_2 in air, in direct contact with the samples (30 mg/well) for 24 and 72 h. Subsequently, 300 μL of NR solution was added to each well. After a 3-h incubation, cells were rinsed with 300 μL of DPBS, and the dye was extracted using 1.5 mL of an ethanol/acetic acid mixture.

The amount of extracted NR was quantified by measuring absorbance at 540 nm using a spectrophotometer (Multiscan RC, Thermolab, Thermo Fisher Scientific, Helsinki, Finland). The absorbance values are directly proportional to cell viability.

2.4.3. MTT assay

The MTT assay (Merck KGaA, Darmstadt, Germany) evaluates cell viability by measuring mitochondrial activity. Viable cells reduce the yellow tetrazolium salt (MTT) to purple formazan crystals via the enzyme succinate dehydrogenase, thereby indicating metabolic activity.

Eluates were prepared by incubating the samples in serum-free DMEM at a ratio of 0.2 g/mL for 72 h at 37 ± 1 °C, in accordance with ISO 10993-12 guidelines. The eluates were subsequently filtered through a 0.22 μm membrane (Merck Millipore, Darmstadt, Germany) to ensure sterility. Cells were cultured in 96-well plates and treated with 50 μL/well of eluates for 24 and 72 h.

After incubation, MTT solution was added to each well and incubated for 4 h. Formazan crystals were then solubilized using dimethyl sulfoxide (DMSO, Merck KGaA, Darmstadt, Germany). Absorbance was measured at 540 nm using a spectrophotometer (Multiscan RC, Thermolab, Thermo Fisher Scientific, Helsinki, Finland). The absorbance values are directly proportional to the cellular metabolic activity, reflecting mitochondrial function.

In both assays, results are expressed as optical density (OD) values. All experiments were performed in triplicate for each sample.

DMEM was used as the negative control (CTRL−), and latex added to DMEM served as the positive control (CTRL+).

2.4.4. Statistical analysis

The results obtained from the cytocompatibility assays were statistically analyzed using One-way ANOVA and Bonferroni [42]post hoc test was performed using GraphPad Prism 9 [43].

3. Results and discussion

3.1. Loading evaluation

The MBGsCe were loaded with polyphenols and drugs. As previously reported [11,20,44], both MBG0 and MBG3.6 showed LC of 0.5–2.0 % and LE of 10.3–39.6 % for the tested polyphenols (Q, F, M, C). Although cerium reduced overall loading, 3.6 mol% offered an effective balance between performance and incorporation efficiency. The loading performance followed the order MBG3.6-Q > MBG3.6-C > MBG3.6-F > MBG3.6-M, with corresponding LC–LE values of 1.2–23.2 %, 1.1–21.9 %, 1.0–20.1 %, and 0.5–10.3 %.

Regarding drug loading, IBU showed markedly higher values (LC: 7.0–10.7 %, LE: 35.4–53.3 %) compared to PARA (LC and LE: 1.0–1.2 %) (Table 1). The presence of cerium slightly decreased these values but did not significantly affect the overall loading performance.

The effect of drug loading was further assessed by measuring the SSA.

Unloaded MBGsCe exhibited high SSA values (300–350 m^2/g) consistent with their mesoporous structure and were unaffected by cerium content. Upon drug loading, a pronounced decrease in SSA was observed due to pore occlusion by the incorporated biomolecules. Specifically, MBG0 showed SSA values of 158 and 255 m^2/g after loading with IBU and PARA, respectively, while MBG3.6 exhibited SSA values of 151 and 246 m^2/g for the same drugs. These results are consistent with previous findings on biomolecule-loaded systems, specifically those incorporating polyphenols, which typically exhibit SSA values of 160–200 m^2/g [9,11].

3.2. Antioxidant activity

Figs. 1 and 2 show the results of the antioxidant activity assays, expressed as the percentage of H_2O_2 decomposed (CAT-like activity) and of the inhibition rate (I.R., SOD-like activity), respectively.

We have demonstrated that CAT-like activity is primarily dependent on the presence of cerium, rather than polyphenols, although a slight CAT-like effect may, in some cases, be attributed to the latter [11].

In this study, we further investigate the potential interference of drugs.

Notably, we confirm once again that cerium enables nearly 100 % CAT-like activity to be achieved within just 30 min, regardless of the specific loading, Fig. 1.

In contrast, we clearly show that SOD-like activity is not influenced by cerium, but is strongly dependent on the presence of polyphenols [11,13,20].

Dual-loaded MBGsCe systems exhibited high SOD-like activity (I.R.:

Table 1
LC (%) and LE (%) calculated for MBGsCe.

	IBU		*PARA*	
	LC (%)	**LE (%)**	**LC (%)**	**LE (%)**
MBG0	10.7	53.3	1.2	1.2
MBG3.6	7.0	35.4	1.0	1.0

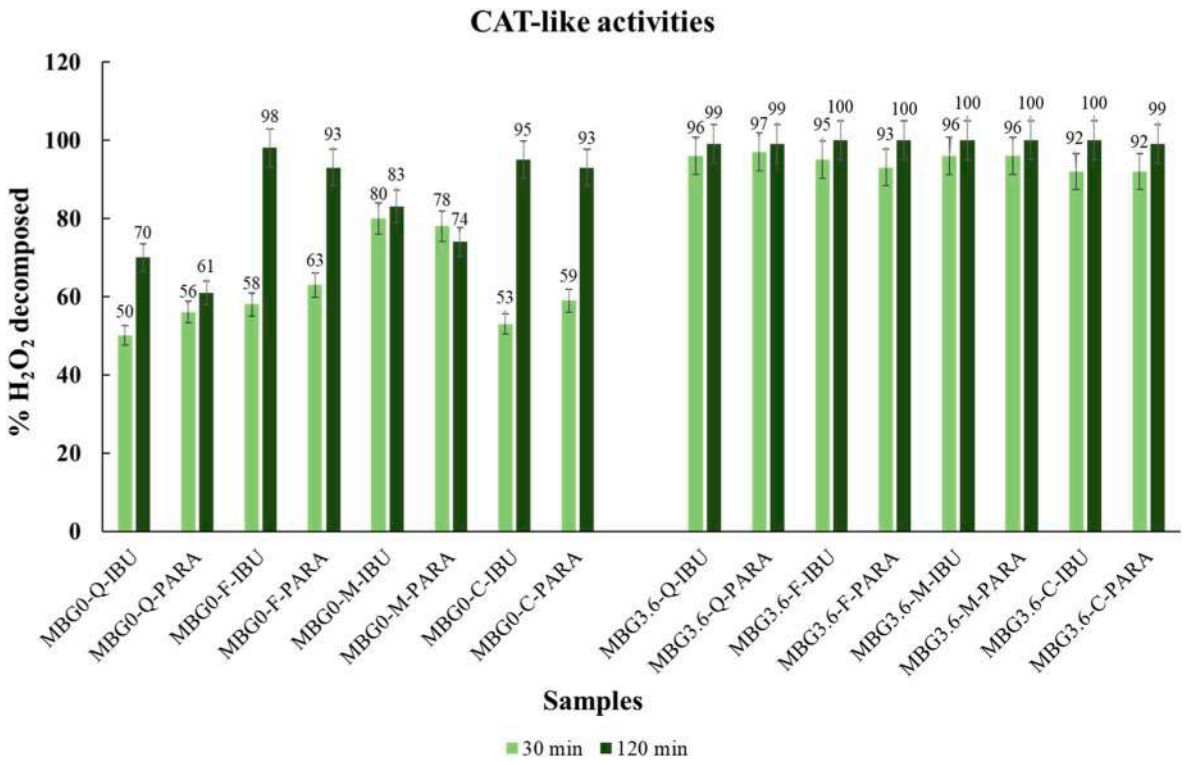

Fig. 1. CAT-like activities of all MBGsCe dual loaded systems expressed as percentage of H_2O_2 decomposed.

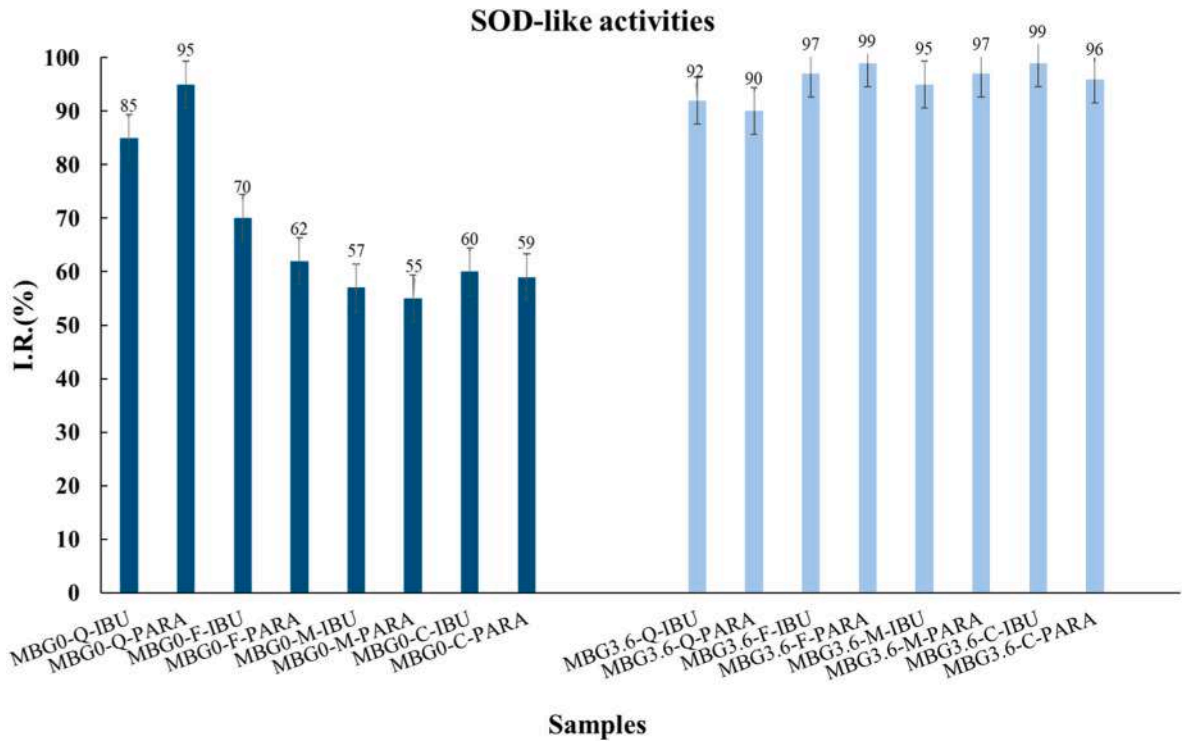

Fig. 2. SOD-like activities of all MBGsCe dual loaded systems expressed as percentage of I.R.

55–99 %), Fig. 2, and this performance was not compromised by the presence of either drug. Interestingly, MBG0 showed lower SOD-like activity than MBG3.6 samples loaded with the same polyphenols.

Figs. 3 and 4 display the SOD-like activity of dual-loaded MBGsCe systems after soaking in DPBS. The SOD-like activity depends on both the polyphenol used and the cerium content.

In our previous study [20] on Q-, F-, and M-loaded MBGsCe, after 48 h in DPBS, the I.R. ranged from 30 to 53 % for MBG0 and 13–37 % for MBG3.6. Co-loading with IBU reduced the I.R. in MBG0 (9–36 %), but maintained or slightly increased it in MBG3.6 (27–38 %). In contrast, co-loading with PARA almost completely suppressed SOD-like activity after 48 h (I.R. 1–5 %), with the exception of MBG3.6-Q-PARA, which

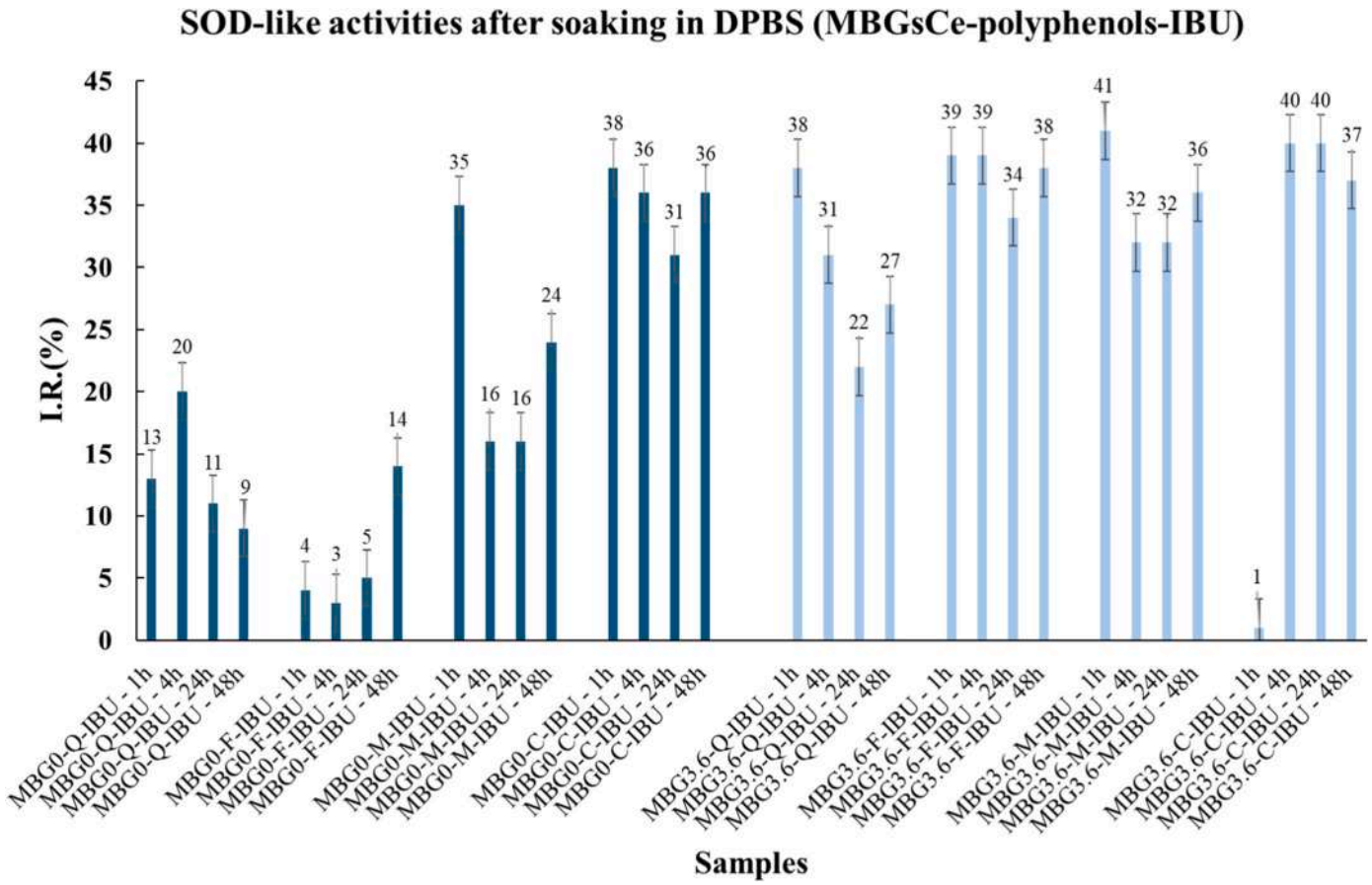

Fig. 3. SOD-like activities of MBGsCe dual loaded systems with POLY and IBU after 1, 4, 24 and 48 h of soaking in DPBS.

retained 13 % activity at that time point.

3.3. In vitro bioactivity assessment

We demonstrated [3,7,20,45], that cerium can be incorporated into glass composition without completely suppressing its bioactivity; cerium tends to delay the formation of an apatite layer by precipitation of cerium-phosphate. We have also shown that polyphenol-loading [11, 20] slows down apatite formation by reducing the available SSA, and we expected a similar effect from the two drugs investigated in this study. For this reason, we extended the soaking times for the bioactivity tests compared to our earlier work.

3.3.1. IBU-loaded MBGsCe

XRPD patterns confirmed the presence of HA through characteristic peaks at 26, 31 and 33 ($^{o}2\theta$), in accordance with JCPDS card No. 00-009-0432 [46].

After 7 days in SBF, all MBG0 systems are bioactive (Fig. 5); in contrast, MBG3.6 systems (Fig. 6) required up to 14 days to develop detectable HA formation. Among these, Q- and F-loaded samples demonstrated robust bioactivity, M-loaded samples showed a modest delay, and C-loaded samples exhibited a pronounced delay.

FTIR spectra (Fig. 7) collected after 7 days (MBG0, panel A) and 14 days (MBG3.6, panel B) in SBF revealed characteristic HA bands at 605 and 565 cm^{-1} [47]. Once again, MBG3.6-C-IBU showed a marked delay in the development of HA bands compared to the other formulations.

SEM analysis of MBG3.6 surfaces after SBF soaking (Fig. 8) revealed spherical HA aggregates on Q-, F-, and M-loaded samples; in contrast, only surface degradation was observed on the C-loaded samples. Table 2 presents the Ca/P molar ratios determined by EDS on the spherical aggregates after 14 days in SBF. All measured ratios approached the stoichiometric HA value of 1.67, confirming the formation of HA layer.

3.3.2. PARA-loaded MBGsCe

PARA dual-loaded MBGs exhibited similar trends, with PARA exerting a stronger inhibitory effect on bioactivity than IBU. Although the MBG0 samples eventually formed an apatite layer after 14 days in SBF, both dual-loading and cerium incorporation increased the induction time required for MBG3.6.

XRPD (Figs. 9 and 10) and FTIR (Fig. 11A and B) analyses confirmed that dual-loading slows, but does not inhibit, HA formation, particularly in MBG3.6 samples.

SEM analysis of MBG3.6-F-PARA (Fig. 12) revealed well-defined spherical HA aggregates. In contrast, M– and Q-loaded samples displayed surface degradation with sparse and small aggregates. The C-loaded sample exhibited minimal surface changes, indicating a markedly delayed bioactivity response. EDS-derived Ca/P molar ratios after 14 days in SBF (Table 2) approached the theoretical HA value of 1.67, further confirming the formation of HA layer.

To provide a clearer interpretation of the data, we included in the Supporting Information the XRPD patterns and FT-IR spectra of unloaded MBG0 and MBG3.6 before (Fig. S1) and after (Fig. S2) 7 and 14 days of SBF soaking.

3.4. Cytocompatibility

Cytocompatibility was evaluated in NIH3T3 cells using NR (Fig. 13) and MTT (Fig. 14) assays. Tests were also performed on materials loaded with individual polyphenols and drugs to obtain a more comprehensive assessment, which had not been carried out before. Previously [22], only type-C polyphenols had been evaluated, and they had shown an improvement in cytocompatibility.

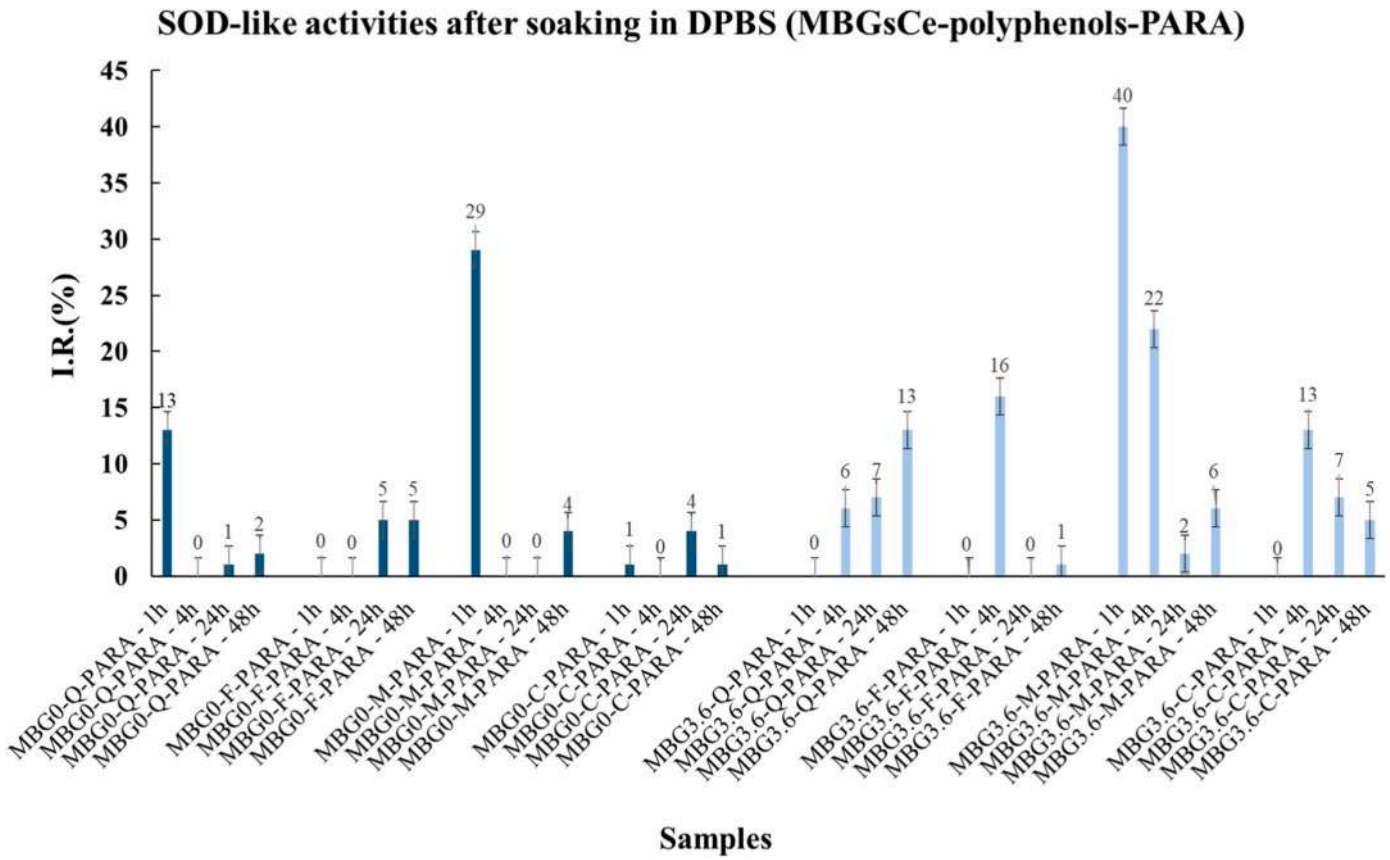

Fig. 4. SOD-like activity of MBGsCe dual loaded systems with POLY and PARA after 1, 4, 24 and 48 h of soaking in DPBS.

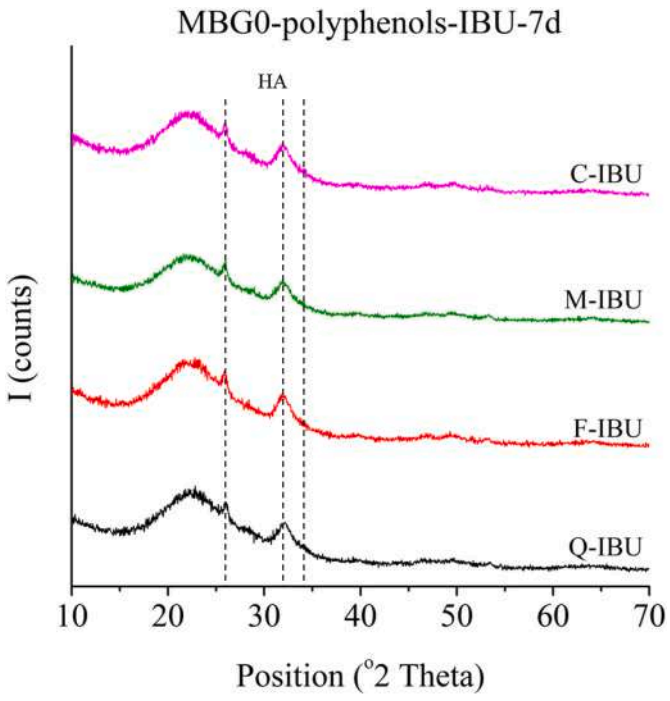

Fig. 5. XRDP patterns of MBG0-Q-IBU, MBG0-F-IBU, MBG0-M-IBU and MBG0-C-IBU after 7 days of soaking in SBF. Dotted lines: HA (26, 31 and 33°2θ).

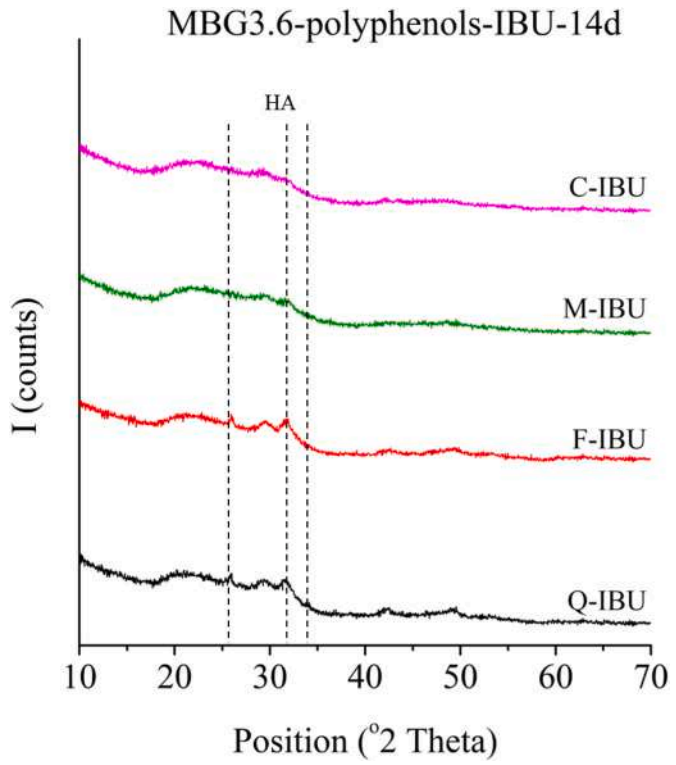

Fig. 6. XRDP patterns of MBG3.6-Q-IBU, MBG3.6-F-IBU, MBG3.6-M-IBU and MBG3.6-C-IBU after 14 days of soaking in SBF. Dotted lines: HA (26, 31 and 33°2θ).

Regarding the dual-loaded systems, the evaluation focused on those containing quercetin and drugs, given that quercetin proved to be one of the most effective and promising polyphenol based on the LC and LE

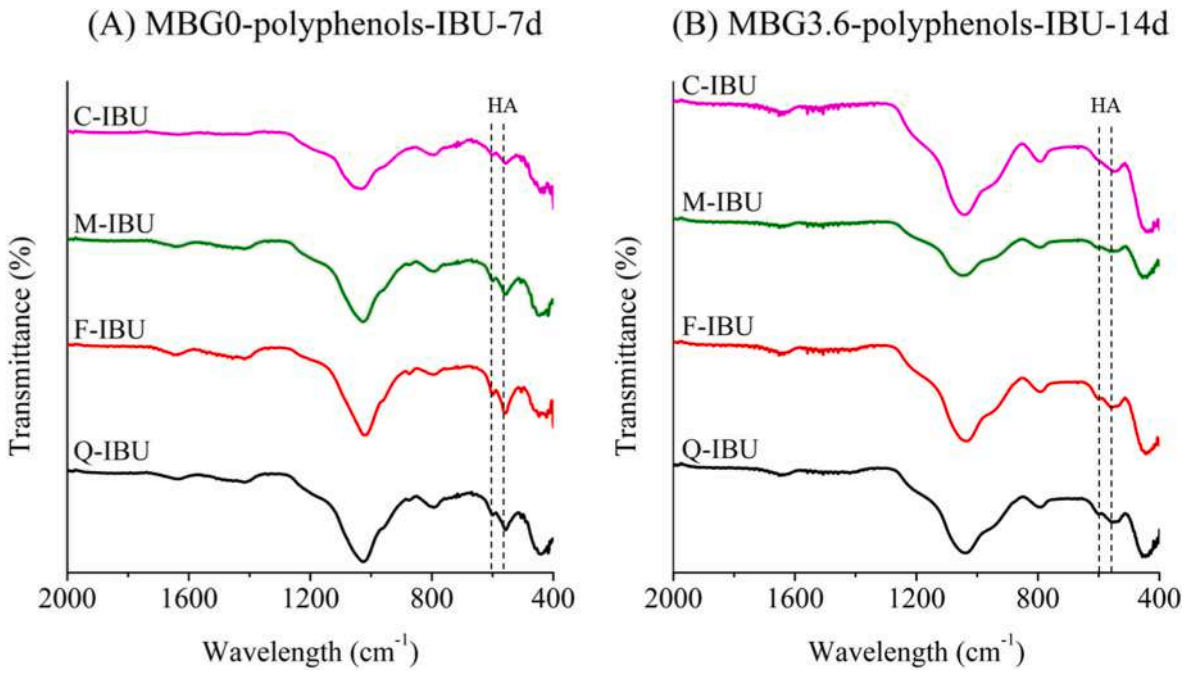

Fig. 7. A. FT-IR spectra of MBG0-Q-IBU, MBG0-F-IBU, MBG0-M-IBU and MBG0-C-IBU after 7 days of SBF soaking. Dotted lines: HA (605 and 565 cm^{-1})
B. FT-IR spectra of MBG3.6-Q-IBU, MBG3.6-F-IBU, MBG3.6-M-IBU and MBG3.6-C-IBU after 14 days of SBF soaking. Dotted lines: HA (605 and 565 cm^{-1}).

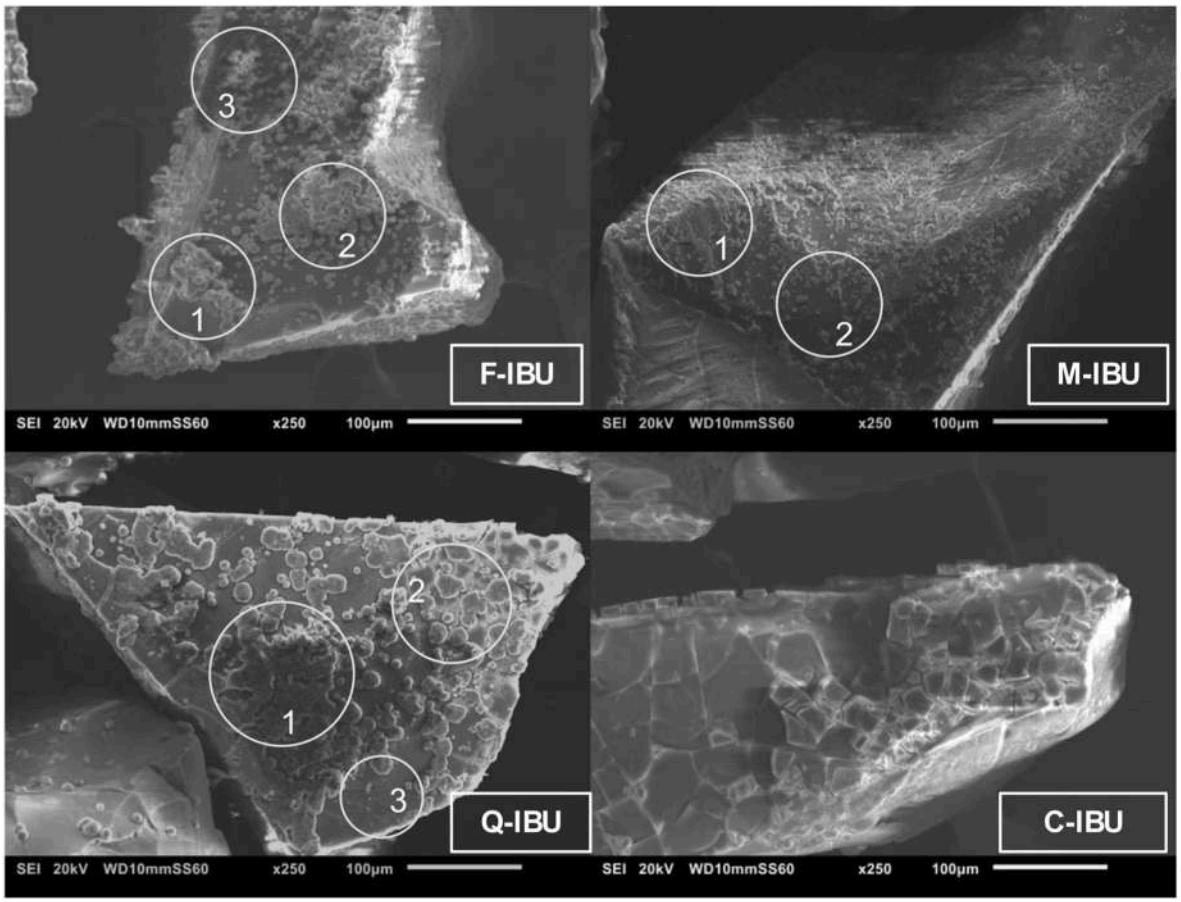

Fig. 8. SEM micrographs of MBG3.6 dual loaded systems after 14 days of SBF soaking.

values.

3.4.1. NR assay

MBG0-Q showed low NR uptake at both 24 and 72 h (59 and 57 %),

Table 2
Ca/P molar ratio of dual loaded MBGs3.6 after 14 days of SBF soaking. The numbers associated with each drug correspond to distinct points analyzed by EDS measurements.

Ca/P	samples
1.57	*F-IBU1*
2.02	*F-IBU2*
1.56	*F-IBU3*
1.86	*M-IBU1*
0.64	*M-IBU2*
1.35	*Q-IBU1*
1.39	*Q-IBU2*
0.74	*Q-IBU3*
1.32	*F-PARA1*
1.13	*F-PARA2*
1.23	*F-PARA3*

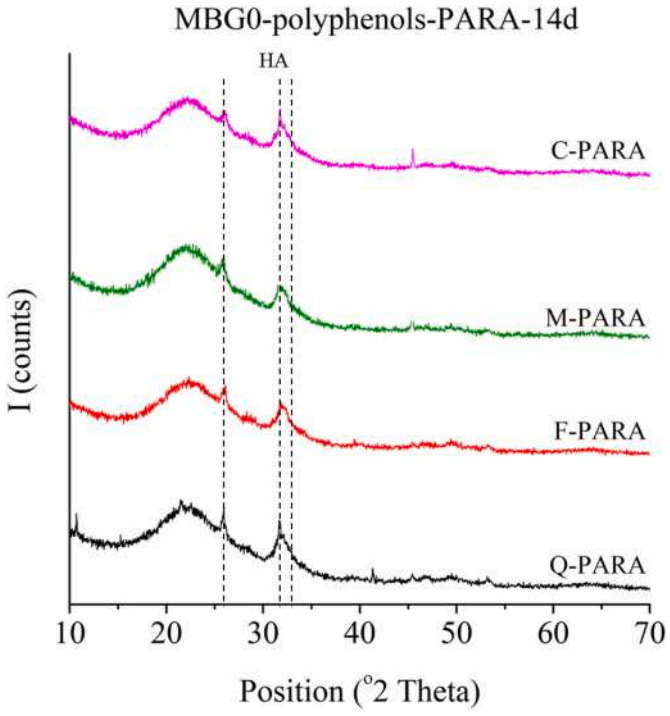

Fig. 9. XRPD patterns of MBG0-Q-PARA, MBG0-F-PARA, MBG0-M-PARA and MBG0-C-PARA after 14 days of SBF soaking. Dotted lines: HA (26, 31 and 33°2*θ)*.

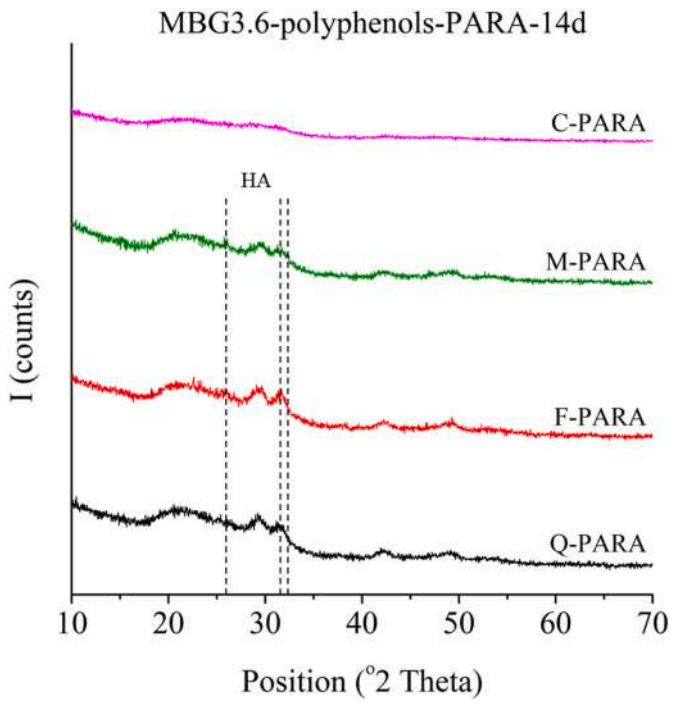

Fig. 10. XRPD patterns of MBG3.6-Q-PARA, MBG3.6-F-PARA, MBG3.6-M-PARA and MBG3.6-C-PARA after 14 days of SBF soaking. Dotted lines: HA (26, 31 and 33°2*θ)*.

suggesting potential cytotoxicity due to rapid or excessive quercetin release. Conversely, MBG3.6-Q exhibited markedly enhanced viability (145 and 140 % at 24 and 72 h, respectively), indicating the synergistic antioxidant and redox-buffering effects of cerium and quercetin, which promote a favourable cellular environment.

For MBG0-F, high viability was observed at 24 h (112 %) but declined at 72 h (61 %), possibly due to depletion of bioactive compounds and the onset of cellular stress. In contrast, MBG3.6-F showed reduced viability at 24 h (63 %) that increased markedly by 72 h (167 %), highlighting a delayed but potent antioxidant effect of cerium oxide, which supports long-term cell survival.

MBG0-M exhibited moderate NR uptake at 24 h (63.0 %), which significantly increased at 72 h (108 %). This suggests an initial cellular adaptation phase followed by enhanced viability, likely supported by the antioxidant properties of morin [12,22,27,28,38–41] that reduce oxidative stress and promote mitochondrial function. In contrast, MBG3.6-M showed high uptake at 24 h (172 %), which decreased substantially by 72 h (61 %). This behaviour is likely due to the rapid release of cerium into the culture medium within the first 24 h, eliciting a strong but transient antioxidant response. As cerium levels decline over time, the cytoprotective effect diminishes, resulting in reduced NR uptake at 72 h.

In all samples, both with and without cerium, the presence of IBU reduced cell viability. However, MBG 3.6-Q-IBU significantly improved viability at both time points (144 and 139 %), likely due to the combined antioxidant and cytoprotective effects of quercetin and cerium, which mitigated IBU induced oxidative stress, preserved mitochondrial integrity, and supported cell metabolism.

In the presence of PARA, cell viability was reduced, with values approaching the cytotoxic threshold at 24 h (48 %), especially for MBG3.6-PARA.

The addition of quercetin in MBG3.6-Q-PARA significantly improved viability (95 and 92 % at 24 and 72 h, respectively), confirming quercetin's potent antioxidant activity in counteracting paracetamol-induced oxidative stress.

3.4.2. MTT assay

The MTT results supported the NR uptake data, reflecting mitochondrial metabolic activity in NIH3T3 cells exposed to the eluates.

MBG0-Q increased cell viability to 140 % at 24 h, which decreased to 87 % at 72 h consistent with the dose- and time-dependent effects of quercetin, which enhances metabolic activity at lower doses but may slightly suppress it with prolonged exposure.

Similarly, MBG3.6-Q showed enhanced mitochondrial activity (131 % at 24 h and 103 % at 72 h), indicating high biocompatibility, likely supported by the synergistic antioxidant properties of cerium and quercetin.

In contrast, MBG0-F and MBG3.6-F showed elevated metabolic activity at 24 h (111 and 106 % respectively), but by 72 h, MBG0-F decreased significantly (60 %), while MBG3.6-F maintained higher activity (86 %) likely due to cerium's ROS-scavenging ability preserving mitochondrial function.

MBG0-M and MBG3.6-M both showed elevated mitochondrial

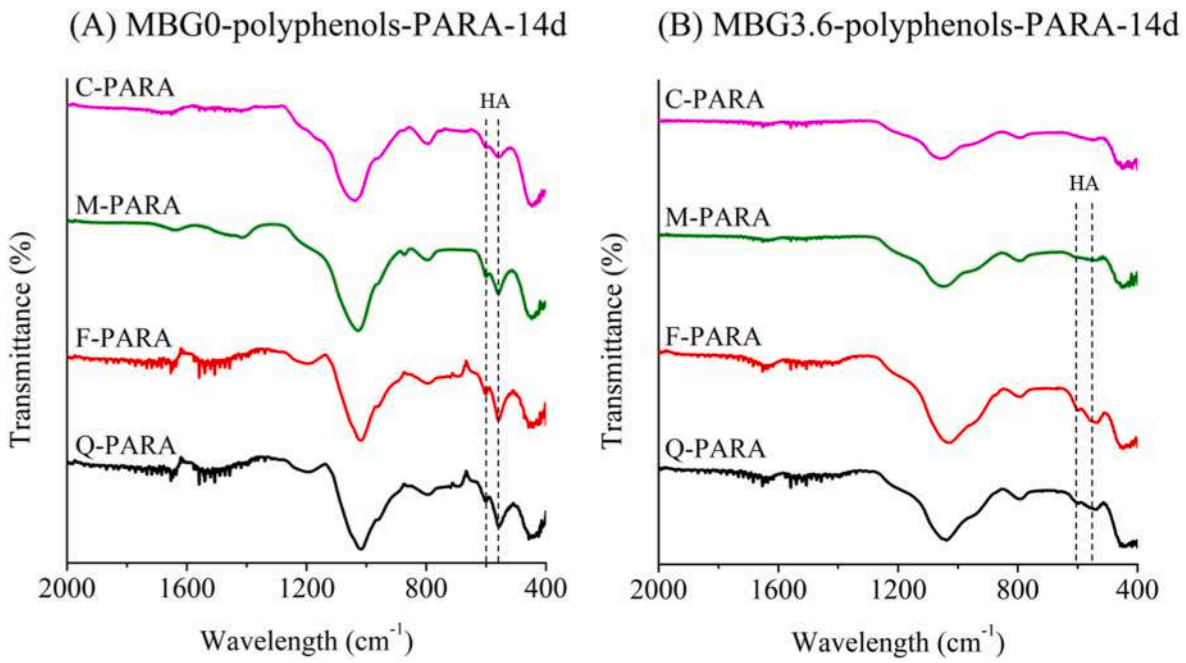

Fig. 11. **A**. FT-IR spectra of MBG0-Q-PARA, MBG0-F-PARA, MBG0-M-PARA and MBG0-C-PARA after 14 days of SBF soaking. Dotted lines: HA (605 and 565 cm^{-1}) **B**. FT-IR spectra of MBG3.6-Q-PARA, MBG3.6-F-PARA, MBG3.6-M-PARA and MBG3.6-C-PARA after 14 days of SBF soaking. Dotted lines: HA (605 and 565 cm^{-1}).

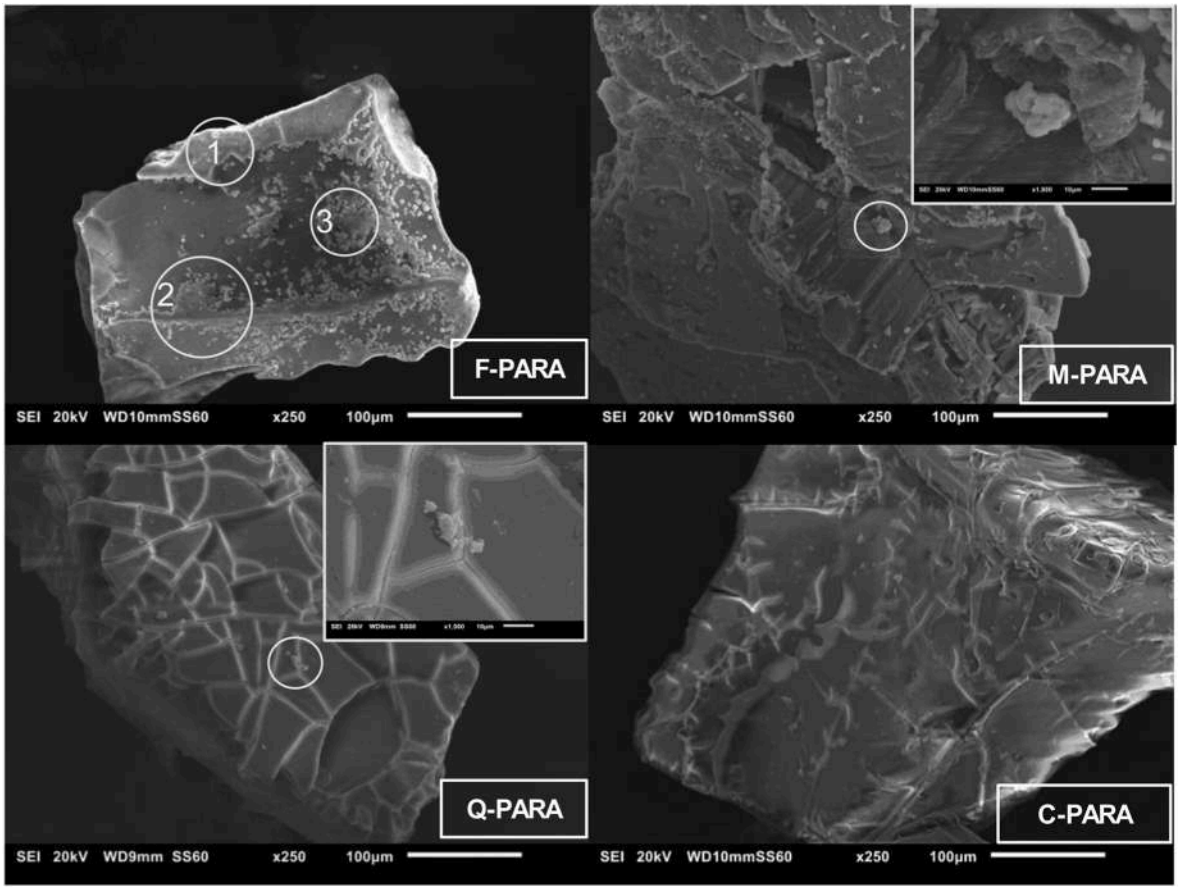

Fig. 12. SEM micrographs of dual-loaded MBG3.6 systems after 14 days of SBF soaking.

activities at 24 h (130 % and 135 %), with sustained levels at 72 h (90 and 104 % respectively), highlighting morin's cytoprotective effect further enhanced by cerium.

MBG3.6-IBU maintained high metabolic activity at both time points (116 and 108 %), suggesting that cerium effectively buffered the negative effects of the drug.

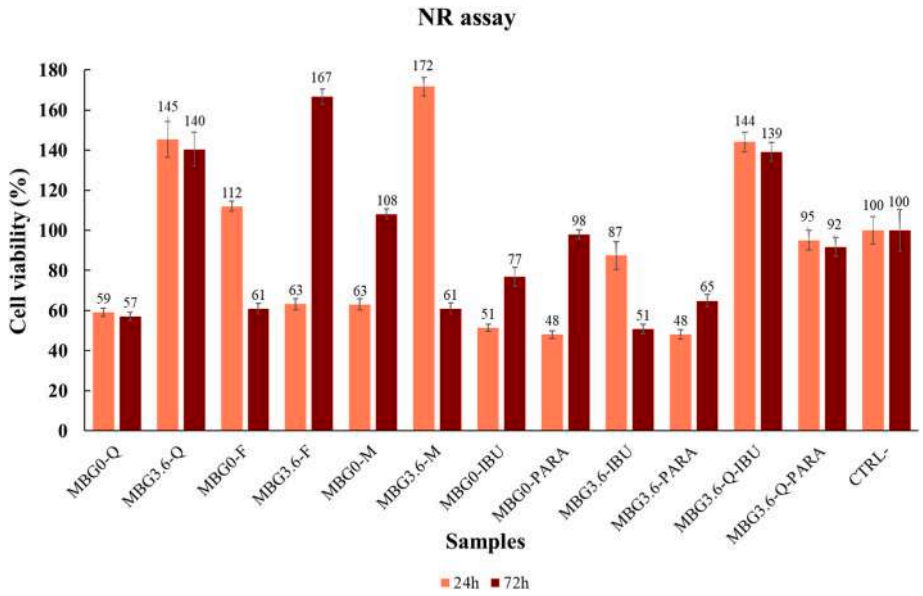

Fig. 13. NR uptake assay of NIH3T3 cells after direct contact of MBGs at 24 and 72 h. Cell viability is related to negative control (CTRL-). Data are mean ± SD (n = 3). Statistical significance was determined using ANOVA with post hoc tests ($p < 0.05$).

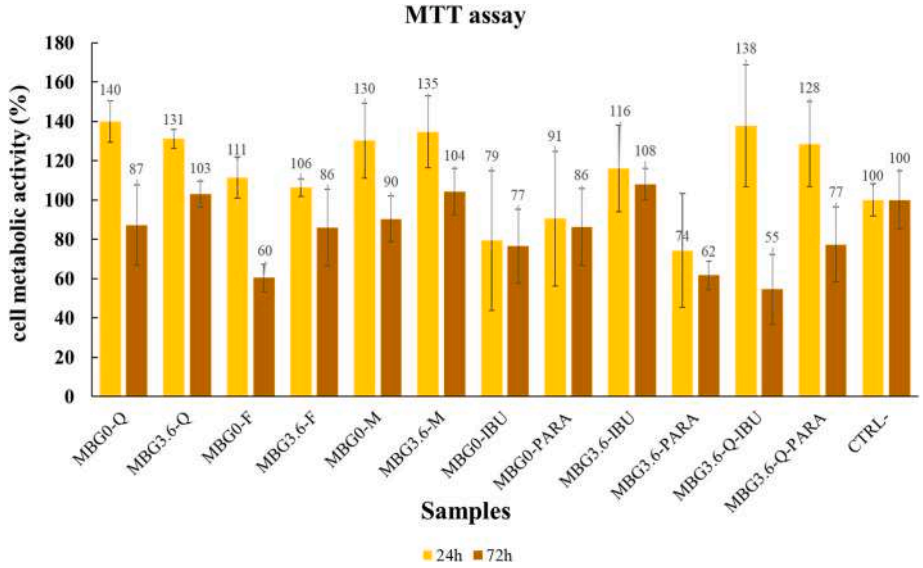

Fig. 14. MTT assay showing mitochondrial activity of NIH3T3 cells after 24 and 72 h to direct contact of MBG's eluates. Cell metabolic activity is related to negative control (CTRL-). Data are mean ± SD (n = 3). Statistical significance was determined by ANOVA ($p < 0.05$).

MBG3.6-PARA samples showed progressively reduced metabolic activity over time (74 % at 24 h and 62 % at 72 h), consistent with paracetamol-induced mitochondrial impairment.

Regarding the dual-loaded samples, MBG3.6-Q-IBU showed high metabolic activity at 24 h (138 %) but fell to 55 % at 72 h, indicating possible time-dependent cytotoxic, effect caused by metabolic overload or drug interactions. MBG3.6-Q-PARA counteracted this decline (128 % at 24 h and 77 % at 72 h), reflecting the partial protective effect of quercetin.

These results strongly corroborate our previous findings, demonstrating that MBGsCe [22] doped with polyphenol type C exhibit remarkably enhanced cytocompatibility, cell viability, and mitochondrial function. The powerful synergistic antioxidant and redox-modulating interplay between cerium and polyphenols markedly reduces oxidative stress and effectively sustains long-term cellular survival and proliferation. In sharp contrast, formulations containing only drugs—without adequate antioxidant support—showed clear signs of cytotoxicity or impaired metabolic activity. These observations underscore the critical importance of controlled dosing and strategic co-doping to ensure optimal biological performance.

The statistical analysis (Table 3) confirms the trends observed in the NR and MTT assays. Most formulations show significant differences compared with the control, reflecting the specific biological impact of each loading strategy. Moreover, the results highlight the synergy between cerium and quercetin, which effectively helps mitigate the cellular stress potentially induced by the drug.

4. Conclusions

This study reports the development of MBGsCe as dual-loaded systems incorporating antioxidant polyphenols (Q, F, M and C) and common drugs (IBU and PARA). The dual-loading strategy aimed to combine

Table 3
One-way ANOVA with Bonferroni post hoc vs CTRL−. Data are presented as mean differences (MD) in viability (% of CTRL−), with pooled-variance t values (df = 91) and Bonferroni-adjusted p values. Significance (s): *p < 0.05; **p < 0.01; ***p < 0.001; ns, not significant.

	NR								MTT							
	24h				72h				24h				72h			
	MD	t	p	s	MD	t	p	s	MD	t	p	s	MD	t	p	s
MBG0-Q	−40.94	−14.71	<0.0001	***	−42.98	−15.63	<0.0001	***	39.87	3.39	0.0123	*	−12.82	−2.05	0.522	ns
MBG3.6-Q	45.41	16.31	<0.0001	***	40.4	14.69	<0.0001	***	31.03	2.64	0.117	ns	2.89	0.46	1	ns
MBG0-F	11.96	4.3	5.2×10^{-4}	***	−39.16	−14.24	<0.0001	***	11.34	0.97	1.0	ns	−39.58	−6.32	1.13×10^{-7}	***
MBG3.6-F	−36.89	−13.25	<0.0001	***	66.73	24.27	<0.0001	***	6.26	0.53	1.0	ns	−14.13	−2.26	0.317	ns
MBG0-M	−36.98	−13.29	<0.0001	***	8.1	2.95	0.049	*	30.18	2.57	0.142	ns	−9.62	−1.54	1	ns
MBG3.6-M	71.65	25.74	<0.0001	***	−39.07	−14.21	<0.0001	***	34.65	2.95	0.0486	*	4.3	0.69	1	ns
MBG0-IBU	−48.7	−17.5	<0.0001	***	−23.12	−8.41	6.5×10^{-12}	***	−20.63	−1.76	0.99	ns	−23.39	−3.74	0.0039	**
MBG0-PARA	−51.96	−18.67	<0.0001	***	−1.98	−0.72	1	ns	−9.48	−0.81	1.0	ns	−13.87	−2.22	0.351	ns
MBG3.6-IBU	−12.57	−4.52	2.3×10^{-4}	***	−49.16	−17.88	<0.0001	***	16.02	1.36	1.0	ns	8.09	1.29	1	ns
MBG3.6-PARA	−51.9	−18.65	<0.0001	***	−35.16	−12.79	<0.0001	***	−25.72	−2.19	0.374	ns	−38.4	−6.13	2.63×10^{-7}	***
MBG3.6-Q-IBU	44.05	15.83	<0.0001	***	39.09	14.22	<0.0001	***	37.63	3.2	0.0225	*	−45.47	−7.26	1.50×10^{-9}	***
MBG3.6-Q-PARA	−4.95	−1.78	0.94	ns	−8.23	−2.99	0.0426	*	−0,0903	2,69	0,33	ns	−22.68	−3.62	0.0058	**

antioxidant activity with therapeutic functionality in a single platform.

Elemental analysis confirmed the successful incorporation of both polyphenols and drugs. For polyphenols, the LC ranged from 0.5 to 2.0 % and the LE from 10.3 to 39.6 %, with the highest values observed for Q.

Among the drugs, IBU exhibited significantly higher loading performance (LC: 7.0–10.7 %; LE: 35.4–53.3 %) compared to PARA (LC and LE: 1.0–1.2 %).

The SSA generally decreased from approximately 300 to 150–250 m^2/g because of partial pore occlusion following molecule incorporation. However, this reduction did not compromise the mesoporous structure, and the presence of cerium had minimal impact on SSA values.

SOD-like activity was evaluated both on powder samples and under release conditions in DPBS. On powders, dual-loaded MBGsCe exhibited high inhibition rates (55–99 %), particularly for MBG3.6, which outperformed the undoped samples. After 48 h in DPBS, SOD activity remained appreciable in ibuprofen-loaded systems, whereas paracetamol induced a marked decrease—except for MBG3.6-Q-PARA, which retained notable activity.

Bioactivity tests confirmed the ability of all dual-loaded systems to induce HA formation in SBF. XRPD and FTIR analyses revealed HA formation after 7 days in MBG0 and after 14 days in MBG3.6, with Ca/P molar ratios approaching the stoichiometric value of 1.67. Although the presence of cerium and the incorporated molecules delayed HA formation, it was not inhibited. Notably, IBU-loaded samples showed more pronounced HA formation compared to PARA-loaded ones.

Importantly, cytocompatibility assays demonstrated good cell viability and mitochondrial activity, particularly in cerium–quercetin systems, reinforcing their suitability for potential clinical translation.

Overall, the results demonstrate that MBGsCe can be effectively co-loaded with antioxidant and pharmacological agents while preserving high antioxidant performance and bioactivity. These dual-loaded systems represent promising candidates for applications in bone regeneration and localized therapy, especially under oxidative or pro-inflammatory conditions.

CRediT authorship contribution statement

Chiara Cavazzoli: Writing – review & editing, Writing – original draft, Investigation, Data curation. **Roberta Salvatori:** Investigation, Data curation. **Alexandre Anesi:** Investigation, Data curation. **Alfonso Zambon:** Writing – review & editing, Writing – original draft, Validation, Supervision, Resources, Methodology, Investigation, Data curation, Conceptualization. **Gigliola Lusvardi:** Writing – review & editing, Writing – original draft, Validation, Supervision, Resources, Methodology, Investigation, Data curation, Conceptualization.

Declaration of competing interest

The authors declare that they have no known competing financial interests or personal relationships that could have appeared to influence the work reported in this paper.

Appendix A. Supplementary data

Supplementary data to this article can be found online at https://doi.org/10.1016/j.ceramint.2025.12.397.

References

[1] L.L. Hench, The story of bioglass®, J. Mater. Sci. Mater. Med. 17 (11) (2006) 967–978, https://doi.org/10.1007/s10856-006-0432-z.
[2] F. Baino, S. Hamzehlou, S. Kargozar, Bioactive glasses: where are we and where are we going? J. Funct. Biomater. 9 (1) (2018) https://doi.org/10.3390/jfb9010025.
[3] A. Zambon, G. Malavasi, A. Pallini, F. Fraulini, G. Lusvardi, Cerium containing bioactive glasses: a review, ACS Biomater. Sci. Eng. 7 (9) (2021) 4388–4401, https://doi.org/10.1021/acsbiomaterials.1c00414.
[4] F. Westhauser, F. Rehder, S. Decker, E. Kunisch, A. Moghaddam, K. Zheng, A. Boccaccini, Ionic dissolution products of cerium-doped bioactive glass nanoparticles promote cellular osteogenic differentiation and extracellular matrix formation of human bone marrow derived mesenchymal stromal cells, Biomed. Mater. 16 (2021), https://doi.org/10.1088/1748-605X/abcf5f.
[5] F. Kurtuldu, N. Mutlu, M. Michálek, K. Zheng, M. Masar, L. Liverani, S. Chen, D. Galusek, A.R. Boccaccini, Cerium and gallium containing mesoporous bioactive glass nanoparticles for bone regeneration: bioactivity, biocompatibility and antibacterial activity, Mater. Sci. Eng. C 124 (2021) 112050, https://doi.org/10.1016/j.msec.2021.112050.
[6] S. Raimondi, A. Zambon, R. Ranieri, F. Fraulini, A. Amaretti, M. Rossi, Investigation on the antimicrobial properties of cerium-doped bioactive glasses, J. Biomed. Mater. Res. 110 (2021), https://doi.org/10.1002/jbm.a.37289.
[7] V. Nicolini, G. Malavasi, A. Zambon, F. Benedetti, G. Cerrato, S. Valeri, P. Luches, Mesoporous bioactive glasses doped with cerium: investigation over enzymatic-like mimetic activities and bioactivity, Ceram. Int. 45 (2019), https://doi.org/10.1016/j.ceramint.2019.07.080.
[8] K. Zheng, J. Kang, B. Rutkowski, M. Gawęda, J. Zhang, Y. Wang, N. Founier, M. Sitarz, N. Taccardi, A.R. Boccaccini, Toward highly dispersed mesoporous bioactive glass nanoparticles with high Cu concentration using Cu/Ascorbic acid

complex as precursor, Front. Chem. 7 (2019), https://doi.org/10.3389/fchem.2019.00497.
[9] M. Miola, Y. Pakzad, S. Banijamali, S. Kargozar, C. Vitale-Brovarone, A. Yazdanpanah, O. Bretcanu, A. Ramedani, E. Vernè, M. Mozafari, Glass-ceramics for cancer treatment: so close, or yet so far? Acta Biomater. 83 (2019) 55–70, https://doi.org/10.1016/j.actbio.2018.11.013.
[10] W. Xia, J. Chang, Well-ordered mesoporous bioactive glasses (MBG): a promising bioactive drug delivery system, J. Contr. Release 110 (3) (2006) 522–530, https://doi.org/10.1016/j.jconrel.2005.11.002.
[11] G. Lusvardi, F. Fraulini, S. D'Addato, A. Zambon, Loading with biomolecules modulates the antioxidant activity of cerium-doped bioactive glasses, ACS Biomater. Sci. Eng. 8 (7) (2022) 2890–2898, https://doi.org/10.1021/acsbiomaterials.2c00283.
[12] R. Salvatori, A. Anesi, L. Chiarini, M. Di Bartolomeo, A. Pellacani, C. Cavazzoli, A. Zambon, G. Lusvardi, Enhanced bone regeneration with cerium-doped bioactive glasses: in vitro and in vivo study, J. Appl. Biomater. Funct. Mater. 23 (2025) 22808000251326790, https://doi.org/10.1177/22808000251326794.
[13] A. Zambon, F. Fraulini, S. Raimondi, Dual loaded Ce-MBGs with bioactivity, antioxidant and antibacterial properties, Ceram. Int. 49 (2023), https://doi.org/10.1016/j.ceramint.2023.06.295.
[14] F. Baino, S. Fiorilli, R. Mortera, B. Onida, E. Saino, L. Visai, E. Verné, C. Vitale-Brovarone, Mesoporous bioactive glass as a multifunctional system for bone regeneration and controlled drug release, J. Appl. Biomater. Funct. Mater. 10 (1) (2012) 12–21, https://doi.org/10.5301/JABFM.2012.9270.
[15] E. Torre, G. Iviglia, C. Cassinelli, M. Morra, Potentials of polyphenols in bone-implant devices, in: J. Wong (Ed.), Polyphenols, IntechOpen, Rijeka, 2018, https://doi.org/10.5772/intechopen.76319 p Ch. 4.
[16] Y. Li, J. Yao, C. Han, J. Yang, M. Chaudhry, S. Wang, H. Liu, Y. Yin, Quercetin, inflammation and immunity, Nutrients 8 (2016) 167, https://doi.org/10.3390/nu8030167.
[17] S. Ali, X. Wang, H.-C. Yan, Morin hydrate: a comprehensive review on novel natural dietary bioactive compound with versatile biological and pharmacological potential, Biomed. Pharmacother. 13 (2021) 111511, https://doi.org/10.1016/j.biopha.2021.111511.
[18] B. Butun, G. Topcu, T. Ozturk, Recent advances on 3-Hydroxyflavone derivatives: structures and properties, Mini Rev. Med. Chem. 17 (2017) 1, https://doi.org/10.2174/1389557517666170425102827.
[19] A. Belščak-Cvitanović, K. Durgo, A. Huđek, V. Bačun-Družina, D. Komes, 1 - overview of polyphenols and their properties, in: C.M. Galanakis (Ed.), Polyphenols: Properties, Recovery, and Applications, Woodhead Publishing, 2018, pp. 3–44, https://doi.org/10.1016/B978-0-12-813572-3.00001-4.
[20] A. Giordana, C. Cavazzoli, F. Fraulini, P. Zardi, A. Zambon, G. Cerrato, G. Lusvardi, Evaluation of the properties of bioactive mesoporous glasses doped with cerium and loaded with polyphenols, Materials 18 (3) (2025), https://doi.org/10.3390/ma18030709.
[21] G. Lusvardi, F. Fraulini, C. Cavazzoli, A. Zambon, Evaluation of the behaviour of hydrogels containing mesoporous glasses doped with cerium and loaded with polyphenols, Ceram. Int. 50 (18) (2024) 33937–33945, https://doi.org/10.1016/j.ceramint.2024.06.213. Part B.
[22] Salvatori, R.; Anesi, A.; Cavazzoli, C.; Zambon, A.; Lusvardi, G. Cytocompatibility of mesoporous bioactive glasses doped with cerium and loaded with polyphenols. J. Am. Ceram. Soc. n/a (n/a), e20395. https://doi.org/https://doi.org/10.1111/jace.20395.
[23] M. Giovannini, M. Mandelli, C. Gualdi, S. Palazzo, Ibuprofen versus steroids: risk and benefit, efficacy and safety, Pediatr. Med. e Chir. 35 (2013) 205–211, https://doi.org/10.4081/pmc.2013.28.
[24] K.D. Rainsford, Ibuprofen: pharmacology, efficacy and safety, Inflammopharmacology 17 (6) (2009) 275–342, https://doi.org/10.1007/s10787-009-0016-x.
[25] A. Bertolini, A. Ferrari, A. Ottani, S. Guerzoni, R. Tacchi, S. Leone, Paracetamol: new vistas of an old drug, CNS Drug Rev. 12 (3–4) (2006) 250–275.
[26] I.K. Ogemdi, A Review on the Properties and Uses of Paracetamol, 2019.
[27] M.V. Berridge, P.M. Herst, A.S. Tan, Tetrazolium dyes as tools in cell biology: new insights into their cellular reduction, in: Biotechnology Annual Review, vol. 11, Elsevier, 2005, pp. 127–152, https://doi.org/10.1016/S1387-2656(05)11004-7.
[28] International Organization for Standardization, Biological Evaluation of Medical Devices —Part 5: Tests for in Vitro Cytotoxicity, 2009. ANSI/AAMI/ISO 10993-52009/(R)2014.
[29] International Organization for Standardization, Biological Evaluation of Medical Devices — Part 12: Sample Prepara- Tion and Reference Materials-ISO 10993-12, 2021.
[30] S. Brunauer, P.H. Emmett, E. Teller, Adsorption of gases in multimolecular layers, J. Am. Chem. Soc. 60 (2) (1938) 309–319, https://doi.org/10.1021/ja01269a023.
[31] I. Celardo, J.Z. Pedersen, E. Traversa, L. Ghibelli, Pharmacological potential of cerium oxide nanoparticles, Nanoscale 3 (4) (2011) 1411–1420, https://doi.org/10.1039/C0NR00875C.
[32] A. Karakoti, S. Singh, J.M. Dowding, S. Seal, W.T. Self, Redox-active radical scavenging nanomaterials, Chem. Soc. Rev. 39 (11) (2010) 4422–4432, https://doi.org/10.1039/B919677N.
[33] F.J. Kelly, Oxidative stress: its role in air pollution and adverse health effects, Occup. Environ. Med. 60 (8) (2003) 612–616, https://doi.org/10.1136/oem.60.8.612.
[34] R. Wetzel, D. Brauer, Apatite formation of substituted bioglass 45S5: SBF vs. Tris, Mater. Lett. 257 (2019) 126760, https://doi.org/10.1016/j.matlet.2019.126760.
[35] T. Kokubo, H. Kushitani, S. Sakka, T. Kitsugi, T. Yamamuro, Solutions able to reproduce in vivo surface-structure changes in bioactive glass-ceramic A-W3, J. Biomed. Mater. Res. 24 (6) (1990) 721–734, https://doi.org/10.1002/jbm.820240607.
[36] A.L.B. Maçon, T. Kim, E. Valliant, K. Goetschius, R. Brow, D. Day, A. Hoppe, A. Boccaccini, I. Kim, C. Ohtsuki, T. Kokubo, A. Osaka, M. Vallet-Regí, D. Arcos, L. Fraile, A. Salinas, A. Teixeira, Y. Vueva, R. Almeida, J. Jones, A unified in vitro evaluation for apatite-forming ability of bioactive glasses and their variants, J. Mater. Sci. Mater. Med. 26 (2015) 5403, https://doi.org/10.1007/s10856-015-5403-9.
[37] M.T. Islam, R.M. Felfel, E.A. Abou Neel, D.M. Grant, I. Ahmed, K.M.Z. Hossain, Bioactive calcium phosphate–based glasses and ceramics and their biomedical applications: a review, J. Tissue Eng. 8 (2017) 204173141771917, https://doi.org/10.1177/2041731417719170.
[38] S. Kumar, A.K. Pandey, Chemistry and biological activities of flavonoids: an overview, Sci. World J. 2013 (1) (2013) 162750, https://doi.org/10.1155/2013/162750.
[39] A.W. Boots, G.R.M.M. Haenen, A. Bast, Health effects of quercetin: from antioxidant to nutraceutical, Eur. J. Pharmacol. 585 (2) (2008) 325–337, https://doi.org/10.1016/j.ejphar.2008.03.008.
[40] R. Salvatori, L. Generali, E. Bellei, S. Bergamini, C. Bertoldi, The inflammation-initiating and resolving mechanisms and oxidation: could periodontal therapy and nutritional strategy improve the systemic health? A narrative review, Food Sci. Nutr. 13 (3) (2025) e70096, https://doi.org/10.1002/fsn3.70096.
[41] R.J. Williams, J.P.E. Spencer, C. Rice-Evans, Flavonoids: antioxidants or signalling molecules? Free Radic. Biol. Med. 36 (7) (2004) 838–849, https://doi.org/10.1016/j.freeradbiomed.2004.01.001.
[42] J.M. Bland, D.G. Altman, Multiple significance tests: the bonferroni method, BMJ 310 (6973) (1995) 170, https://doi.org/10.1136/bmj.310.6973.170.
[43] GraphPad Prism version 6.04 for Windows, GraphPad Software, Boston, Massachusetts USA, www.graphpad.com.
[44] C. Cavazzoli, F. Fraulini, V. Nicolini, P. Zardi, E. Busi, S. Raimondi, A. Zambon, G. Lusvardi, Double-ion doped mesoporous glasses: studies on stability, antibacterial and antioxidant properties, and bioactivity, Surf. Interfaces 72 (2025) 106954, https://doi.org/10.1016/j.surfin.2025.106954.
[45] C. Leonelli, G. Malavasi, L. Menabue, M. Tonelli, Synthesis and characterization of cerium-doped glasses and in vitro evaluation of bioactivity, J Non-Cryst Solids 316 (2003) 198–216, https://doi.org/10.1016/S0022-3093(02)01628-9. Journal of Non-crystalline Solids.
[46] S. Gates-Rector, T. Blanton, The powder diffraction file: a quality materials characterization database, Powder Diffr. 34 (2019) 1–9, https://doi.org/10.1017/S0885715619000812.
[47] C. Drouet, Apatite formation: why it may not work as planned, and how to conclusively identify apatite compounds, BioMed Res. Int. 2013 (2013) 490946, https://doi.org/10.1155/2013/490946.